International Journal of Mechanical, Industrial and Aerospace Sciences
ISSN: 2517-9950
Vol:10, No:1, 2016

Reducing Pressure Drop in Microscale Channel Using Constructal Theory

K. X. Cheng, A. L. Goh, K. T. Ooi

***Abstract*—**The effectiveness of microchannels in enhancing heat transfer has been demonstrated in the semiconductor industry. In order to tap the microscale heat transfer effects into macro geometries, overcoming the cost and technological constraints, microscale passages were created in macro geometries machined using conventional fabrication methods. A cylindrical insert was placed within a pipe, and geometrical profiles were created on the outer surface of the insert to enhance heat transfer under steady-state single-phase liquid flow conditions. However, while heat transfer coefficient values of above 10 kW/m^2·K were achieved, the heat transfer enhancement was accompanied by undesirable pressure drop increment. Therefore, this study aims to address the high pressure drop issue using Constructal theory, a universal design law for both animate and inanimate systems.

Two designs based on Constructal theory were developed to study the effectiveness of Constructal features in reducing the pressure drop increment as compared to parallel channels, which are commonly found in microchannel fabrication. The hydrodynamic and heat transfer performance for the Tree insert and Constructal fin (Cfin) insert were studied using experimental methods, and the underlying mechanisms were substantiated by numerical results. In technical terms, the objective is to achieve at least comparable increment in both heat transfer coefficient and pressure drop, if not higher increment in the former parameter.

Results show that the Tree insert improved the heat transfer performance by more than 16 percent at low flow rates, as compared to the Tree-parallel insert. However, the heat transfer enhancement reduced to less than 5 percent at high Reynolds numbers. On the other hand, the pressure drop increment stayed almost constant at 20 percent. This suggests that the Tree insert has better heat transfer performance in the low Reynolds number region. More importantly, the Cfin insert displayed improved heat transfer performance along with favourable hydrodynamic performance, as compared to Cfin-parallel insert, at all flow rates in this study. At 2 L/min, the enhancement of heat transfer was more than 30 percent, with 20 percent pressure drop increment, as compared to Cfin-parallel insert. Furthermore, comparable increment in both heat transfer coefficient and pressure drop was observed at 8 L/min. In other words, the Cfin insert successfully achieved the objective of this study.

Analysis of the results suggests that bifurcation of flows is effective in reducing the increment in pressure drop relative to heat transfer enhancement. Optimising the geometries of the Constructal fins is therefore the potential future study in achieving a bigger stride in energy efficiency at much lower costs.

Cheng K. Xian is with School of Mechanical and Aerospace Engineering, Nanyang Technological University, 50 Nanyang Avenue, Singapore 639798 (phone: +6591157260, e-mail: kcheng003@e.ntu.edu.sg).

Goh A. Ling is with Interdisciplinary Graduate School, Nanyang Technological University, 50 Nanyang Drive, Singapore 637553 (e-mail: agoh006@e.ntu.edu.sg).

Ooi K. Tiow is with School of Mechanical and Aerospace Engineering, Nanyang Technological University, 50 Nanyang Avenue, Singapore 639798 (e-mail: mktooi@e.ntu.edu.sg).

***Keywords*—**Constructal theory, enhanced heat transfer, microchannel, pressure drop.

I. Introduction

THE miniaturisation and enhanced performance of electronic devices call for more effective methods to remove the heat produced, ensuring the optimal performance and material integrity of the devices. In order to cater for the spiralling demand in terms of heat transfer, Tuckerman and Pease [1] introduced micro-channel heat sinks in 1981. Their work has spawned numerous studies in microscale heat sinks as reviewed by [2]. Reference [3] reported that microscale heat sink has a heat dissipation capacity of 1000 W/cm^2 at a maximum surface temperature of 120˚C. The milestone achieved by microscale heat sinks has motivated the continuous studies on this subject matter, and it is still panning out in an encouraging manner hitherto.

Although microscale level heat transfer has depicted great potential in microelectronic devices, its presence in macro geometries is uncommon, attributable to both technological and cost constraints. In order to tap on the augmented microscale heat transfer in macro geometries, [4] proposed the implementation of microscale heat transfer in macro geometries by using conventional methods, having a competitive advantage in terms of manufacturability and costs. Furthermore, this nascent technology achieved a heat transfer coefficient exceeding 10 kW/m^2·K which is not common in macro geometries. The study placed an insert concentrically into a circular channel to simulate the microscale heat transfer, having nominal gap size of 1000 μm to 300 μm. The study yielded convincing results on the feasibility to tap the augmentation of heat transfer in microchannels into macro geometries with sevenfold heat transfer coefficient enhancement, corroborated by both numerical and experimental investigations.

A number of studies [5], [6] were performed to improve the heat transfer in microchannels by introducing geometrical features. Fins and wavy surfaces were introduced to beef up the thermal performance of microchannels. A study [7] showed that geometrical features pumped up the heat transfer coefficient by 100 times in comparison to the plain ones, while the pumping power was only increased by four times. Motivated by the positive results achieved by enhanced heat transfer in microchannels, Goh et al. [8] configured several surface features in the microscale heat transfer region in macro geometries. Both numerical and experimental approaches had been attempted to examine the effect of the surface profile on heat transfer and pressure drop. Although the heat transfer had

been beefed up, the increase in pressure drop exceeded the improvement in heat transfer, based on percentage basis. This does not bode well with the full implementation of enhanced microscale heat transfer in macro geometries, as the vexed problem of pressure drop implies higher pumping requirement. This contradicts the ultimate aim of implementation of microscale heat transfer in macro geometries, promoting energy efficiency. At this juncture of the implementation of microscale heat transfer in macro geometries, addressing the hydrodynamic woes becomes as crucial as the enhancement in the heat transfer before this technology makes its debut in engineering devices or systems. This study aims to address the undesirable plunge in pressure across the heat transfer region.

This study delves into the design of the inserts of 19.4 mm nominal diameter to be placed concentrically into a circular pipe with an internal diameter of 20 mm, creating an annular microchannel of 0.3 mm. Constructal law, a principle introduced in 1996 [9] to justify the universal "design" physical phenomenon, is adopted in designing the configurations and dimensions of the inserts. The rules and principles that form the universal flow systems, both animate and inanimate, are applied in this study in order to minimise the inherited flow resistance that comes with the geometrical features on the inserts.

Wechsatol et al. [10] studied the optimised geometric layout for uniform distribution of hot water, subjected to constraints such as materials and piping volume. It was found that tree designs outperformed the coiled stream design. Furthermore, the study suggested that optimised tree-shaped flow designs were better than those which were not optimised at each level. In other words, optimised tree-shaped flow designs were robust.

Bejan [11] discussed the application of Constructal law on counter flow channels as shown in Fig. 1. Cold and hot fluid was channelled through the upper and lower surface respectively. The performance was compared with parallel channels shown in Fig. 2. The analysis was supported by a numerical study [12]. Both studies achieved a higher percentage increment in heat transfer as compared to the percentage increment in pressure drop despite the constant discrepancies attributable to a number of factors highlighted in the paper. The heat transfer and hydrodynamic performance of the tree channels were better than parallel channels only under certain circumstances which were affected by channel depth, svelteness, volumetric fraction, number of pairing of trees and so on.

Chen et al. [14] did experimental and numerical comparison on Constructal tree-shaped network and serpentine flow pattern in minichannel heat sink. Both methodologies showed similar result and they proved that Constructal tree-shaped network had an upper hand in terms of heat transfer and pressure drop. In addition, they found out that diffluence tree network has lower pressure drop compared to confluence one.

Although the improvement of both heat transfer and hydrodynamic performance simultaneously is not feasible, the study targets a relatively lower percentage drop in pressure in comparison to the increment in the heat transfer coefficients.

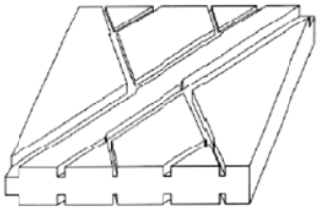

Fig. 1 Line-to-line tree channels in counterflow [13]

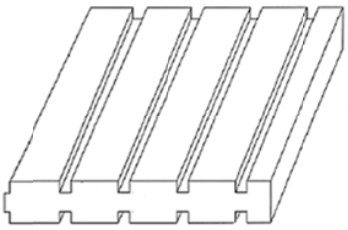

Fig. 2 Two sets of parallel channels in counterflow [13]

II. Experimental Setup and Procedures

A. Experimental Setup

Fig. 3 shows the setup for the experiment. The major components of this setup include the flow loop, chiller, filter, test module, measuring devices, and data acquisition system.

The flow loop consists of test loop, by-pass loop and air-vent loop. Water at the desired inlet temperature to the test module is circulated from a reservoir in the chiller to the flow loop by a positive displacement pump. The amount of water entering the test loop is controlled by a needle valve whereas the remaining flow returns to the reservoir through the by-pass loop. The air-vent loop removes any bubbles in the flow.

The water is channelled through a 40 micron filter to remove solid particles before entering the test module to remove the heat generated in the test module. Total flow into the test module is first controlled using the by-pass needle valve before further controlled by the additional needle valve downstream of the test module. The flow rate is measured using Coriolis flow meter. In order to measure the key parameters, the temperature and pressure sensors are installed at the entrance and exit of the test module. The test loop flow is subsequently channelled back to the chiller to be cooled and re-circulated. Ensure uniform distribution of the flow in the circumferential direction at the entrance of the channel. The copper block with heater served as the heat source for this experiment. It was capable of supplying heat rate up to 3000 W. Heat loss was reduced by using PEEK pipe and mica as an insulating cover.

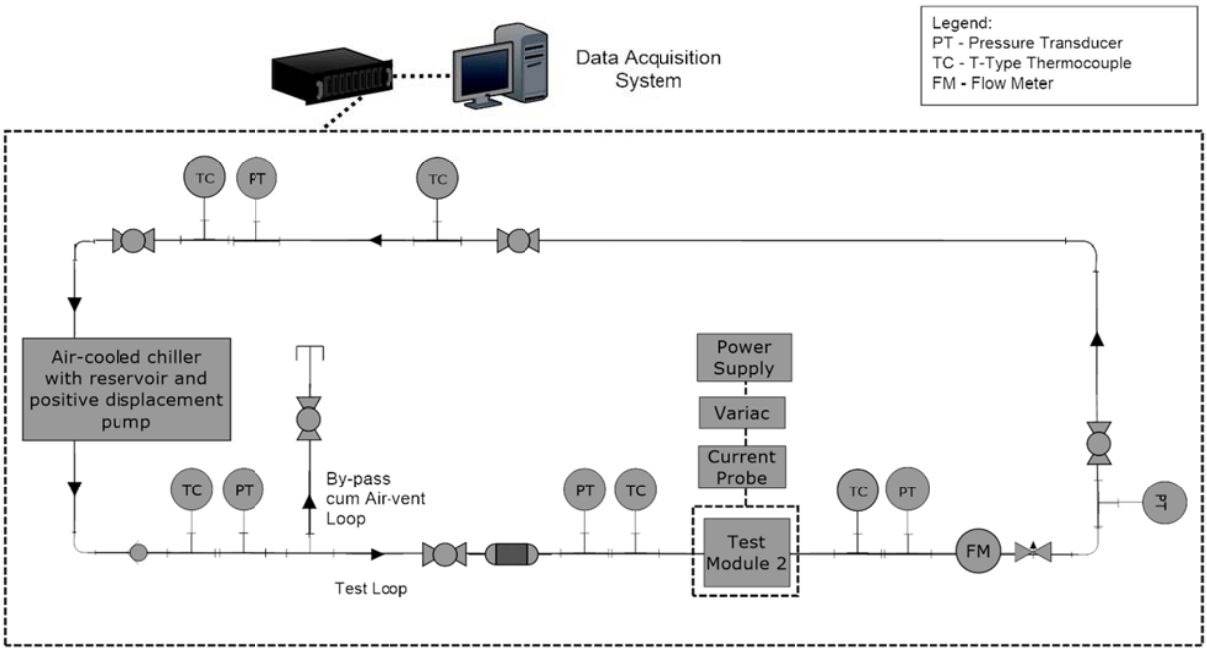

Fig. 3 Experimental test bed

B. Experimental Test Module

Fig. 4 and Fig. 5 show the front view and the cross sectional view of the test module. It consists of a copper block with heater, a stainless steel insert, two insert holders, two polyether ketone (PEEK) pipes and mica insulating cover. The annular microchannel of length 30 mm was formed by the outer surface of the insert and the inner surface of the copper block. An insert of nominal diameter 19.4 mm was inserted concentrically into the copper block which has an inner diameter of 20 mm, forming a microchannel with hydraulic diameter 0.6 mm or 600 µm. Two insert holders manufactured with small tolerances were used to ensure the concentricity of the insert. Sufficient length of PEEK pipe which was 70 mm in this experiment was placed in front of the annular channel to ensure uniform distribution of the flow in the circumferential direction at the entrance of the channel. The copper block heater served as the heat source for this experiment. It was capable of supplying heat up to 3000 W. Heat loss was reduced by PEEK pipe and mica as insulating cover.

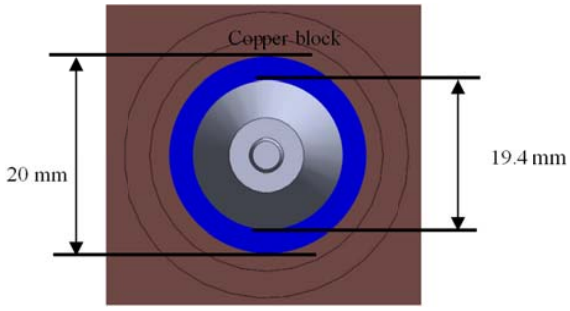

Fig. 4 Front view of the flow channel

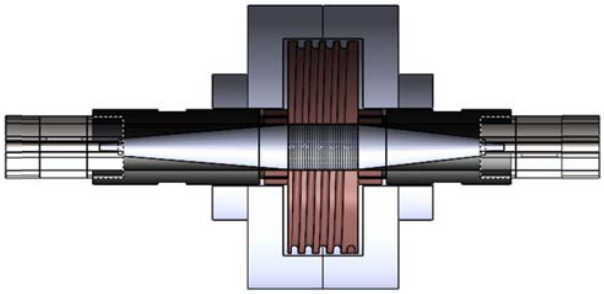

Fig. 5 Sectional view of the test moduleInsert design

Different surface profiles were fabricated onto the surface of the highlighted region in Fig. 6 to perturb the flow, keeping the flow in the developing region.

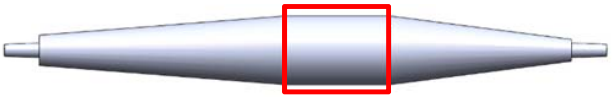

Fig. 6 Insert

There were a total of four different surface profiles designed for the insert, giving rise to Tree insert, Tree-parallel insert, Cfin insert and Cfin-parallel insert as shown in the Figs. 7-10. The design parameters are summarised in Tables I and II.

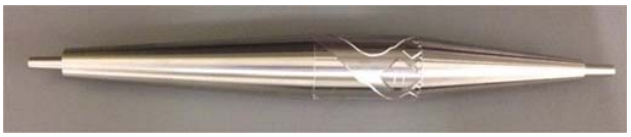

Fig. 7 Tree insert

Fig. 8 Tree-parallel insert

Fig. 9 Cfin insert

Fig. 10 Cfin-parallel insert

TABLE I
KEY PARAMETERS OF TREE AND TREE-PARALLEL INSERTS

	Tree	Tree-parallel
Volume of insert (mm^3)	8865.66	8865.66
Nominal diameter (mm)	19.40	19.40
Volume of fluid on the surface of the insert (mm^3)	130.56	130.56
Maximum diameter (mm)	19.54	19.54
Channel depth (mm)	0.20	0.20
Total volume of fluid in microchannel (mm^3)	559.12	559.12

TABLE II
KEY PARAMETERS FOR CFIN AND CFIN-PARALLEL INSERTS

	Cfin	Cfin-parallel
Volume of insert (mm^3)	8863.65	8864.39
Nominal diameter (mm)	19.40	19.40
Volume of fluid on the surface of the insert (mm^3)	241.81	241.07
Maximum diameter (mm)	19.66	19.66
Channel depth (mm)	0.20	0.20
Total volume of fluid in microchannel (mm^3)	561.13	560.39

An insert with parallel channels was created to compare the performance between tree designs and parallel channels. The nominal diameter and the total volume of fluid in the microchannel were the same for both cases for fair comparison.

C. Measuring Devices

Both J-type and T-type thermocouples were used in this experiment for temperature measurement. Covering the whole range of water temperature and having lower tolerances, T-type thermocouples were used to measure water temperature in this experiment. Two of them were installed before and after the test module whereas the other three were spread out over the flow loop for monitoring purposes. J-type thermocouples, on the other hand, were installed in the test module to measure copper temperature. Five of these thermocouples were installed on opposite side of the module to measure the surface temperature of the test module. The additional two out of twelve that were present in the test module were placed at a depth of 5 mm from the copper outer surface, sending feedback signal to data acquisition system and circuit breaker at high heater temperature.

A total of five pressure transducers were used. Two of them were placed before and after the test module to measure the pressure drop whereas the other three were spread out over the flow loop for monitoring purposes. The pressure transducers used were WIKA model A-10, giving current signals of 4 to 20 mA, corresponding to pressure readings of 0 to 6 barg. The allowed temperature range of the medium was 0 to 80℃. Coriolis flowmeter was used to measure the flow rate.

D. Data Reduction

The data obtained from the 10-minute steady state data collection process was then processed to obtain the average heat transfer coefficient h using Newton's law of cooling as shown in (1):

$$h = \frac{\dot{Q}}{A\left(T_{w,m} - T_{f,m}\right)} \tag{1}$$

The heat rate was deduced from the temperatures obtained from the inlet and outlet of the test module as shown in (2). The mass flow rate, $\dot{m}$ was obtained by multiplying the density of water by the flow rate. All the fluid properties used in the calculations were taken from National Institute of Standards and Technology (NIST) Reference Fluid and Thermodynamic and Transport Properties Database (REFPROP). The variation of the properties due to temperature was taken into consideration in the experiment.

$$\dot{Q} = \dot{m}\left(C_{p,out}T_{out} - C_{p,in}T_{in}\right) \tag{2}$$

The wall temperature, T_w was obtained by considering the cylindrical solid conduction in the copper block. As the temperature acquired by the thermocouples were at a radial distance away from the wall, T_w was approximated using (3). The fluid temperature, T_f on the other hand, was calculated by taking the average of inlet and outlet temperature of the fluid.
The pressure drop was deduced from the pressure difference taken at the inlet and outlet of the test module, as shown in (4).

$$T_{w,i} = T_{r,i} - q\frac{\ln(d_r / d_w)}{2\pi L k_c} \tag{3}$$

$$\Delta P = P_{out} - P_{in} \tag{4}$$

Equations (5) and (6) show the calculation of Reynolds number and Nusselt number respectively.

$$\mathrm{Re} = \frac{\dot{m}D_h}{A_c\mu} \tag{5}$$

$$Nu = \frac{hD_h}{k_f} \quad (6)$$

The hydraulic diameter, D_h was evaluated using hydraulic diameter for annular channels and the nominal diameter of the insert was taken as the inner diameter.

$$D_h = D_o - D_i \quad (7)$$

E. Experimental Conditions

All the four inserts were tested under different flow rates with the same amount of heat supply.

TABLE III summarises the operating conditions.

TABLE III
OPERATING CONDITIONS FOR EACH EXPERIMENTAL RUN

Experiment run	Flow rate (L/min)	Heat supply (W)
1	2.00	1000
2	3.00	1000
3	4.00	1000
4	5.00	1000
5	6.00	1000
6	7.00	1000
7	7.50	1000

F. Uncertainty Range

The maximum uncertainty values for heat transfer coefficient, Nusselt number, Reynolds number and pressure drop across test module were estimated in percentage and tabulated in Table IV. These values were expressed as error bars for the result analysis.

TABLE IV
MAXIMUM UNCERTAINTY VALUES

Parameter	Maximum uncertainty (%)
Heat transfer coefficient	7.6
Nusselt number	7.7
Reynolds number	0.5
Pressure drop across test module	10.2

III. COMPUTATIONAL METHOD

Computational approach was used to back up the experimental results while providing insights of the fluid flow, visualizing the fluid flow from velocity and streamlines from the post processing of results. In this project, 3D model was employed due to the non-symmetrical surface profile on the insert and solved using the commercially available software, ANSYS CFX.

A. Governing Equations and Boundary Conditions

In this project, the steady-state conjugate heat transfer problem was employed to account for the thermal heat conduction in the solid regions and convection in the fluid regions. The governing equations [15] which include continuity, momentum and thermal energy equations were solved numerically, as listed in (8)-(11).

Continuity equation for the fluid domain:

$$\nabla \cdot \left(\rho_f U_f \right) = 0 \quad (8)$$

Momentum equation for the fluid domain:

$$\nabla \cdot \left(\rho_f U_f \otimes U_f \right) = -\nabla P + \nabla \cdot \tau + S_{M,f} \quad (9)$$

where the stress tensor τ is defined as:

$$\tau = \mu \left[\nabla U + (\nabla U)^T - \frac{2}{3} \delta \nabla \cdot U \right]$$

Thermal energy equation for the fluid domain:

$$\nabla \cdot \left(\rho_f U_f h_{e,f} \right) = \nabla \cdot \left(k_f \nabla T_f \right) + S_{E,f} \quad (10)$$

Thermal energy equation for the solid domain:

$$\nabla \cdot \left(\rho_s U_s h_{e,s} \right) = \nabla \cdot \left(k_s \nabla T_s \right) + S_{E,s} \quad (11)$$

The equations were solved using the boundary conditions as presented. The boundary conditions at the various locations are as follows:

a. Flow inlet: The flow at inlet was assumed a uniform velocity with a volumetric flow rate of 4 L/min at a mean temperature of 28℃.
b. Flow outlet: The atmospheric pressure which is 101 kPa was assumed.
c. Heat source: The heating coils were modelled as uniform volumetric heating with heat supply of 1000 W.
d. Solid-solid and solid-fluid interfaces: The temperature and heat flux were treated to be continuous at the solid walls and the solid-liquid contact surfaces.
e. Outermost surfaces: The heat loss from the assembly was assumed to be happening at outermost surfaces of mica insulation, PEEK pipes and insert holders. The surrounding temperature was set at 28°C, using a heat transfer coefficient of 8 W/m^2·K, based on the approximation from [4].
f. The International Association for Properties of Water and Steam (IAPWS) standards was used to account for the thermophysical variation of the water. The solid materials include copper, stainless steel, mica and polyether ether ketone were assumed constant solid properties at 28°C.

IV. RESULTS AND DISCUSSION

A. Tree Series Insert

Fig. 11 shows the variation of heat transfer coefficients for Tree series with flow rate. It can be seen from the graph that the heat transfer coefficient for all the inserts increases with flow rate. The Plain insert achieves a heat transfer coefficient of 10 kW/m^2·K at 2 L/min flow rate, achieving the heat removal capability of a microchannel. The Tree insert results in higher heat removal capability as compared to the other two inserts, particularly at low flow rate. The improvement at higher flow rates is insignificant as compared to the Tree-

parallel insert as the heat transfer coefficient falls into the uncertainty range. The highest heat transfer coefficient is close to 30 kW/m^2·K, achieved by the Tree series at 8 L/min flow rate.

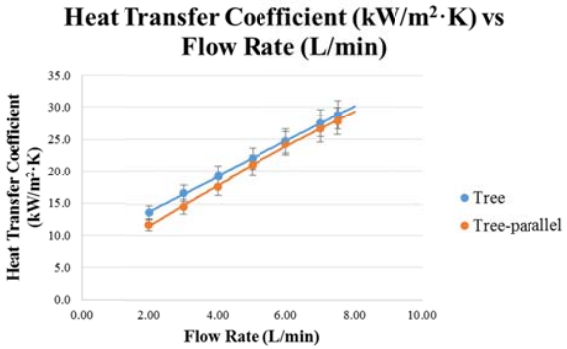

Fig. 11 Variation of heat transfer coefficient with flow rate

The results in Fig. 11 are summarised in dimensionless numbers as shown in Fig. 12. It can be seen from the graph that Tree insert is better than Tree-parallel insert in enhancing the heat transfer coefficient at low Reynolds number. Beyond that, the augmentation achieved by both inserts is similar. This phenomenon is expected as the surface geometry on the insert initiates flow development and thus taps into the high heat transfer in the developing region. As the flow rate increases, the flow turns disorder. Eddies and vortices promote liquid mixing and thus escalating the heat transfer process of the liquid in the radial direction. At high flow rates, the flow enters the turbulence regime. The initiation of turbulence region by the surface grooves causes little improvement to the heat transfer.

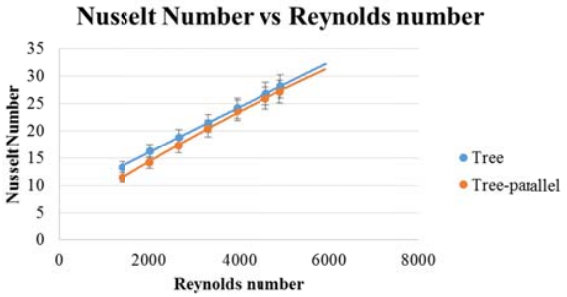

Fig. 12 Variation of Nusselt number with Reynolds number

Fig. 13 shows the variation of pressure drop of Tree series inserts with flow rate. At low flow rates, all the inserts have similar magnitude of pressure drop, less than 0.2 bar at 2 L/min. However, the magnitude of pressure drop increases with the increase in flow rate, although each insert has different rate of increase. Tree insert suffers the highest rate of pressure loss increment, achieving 1.40 bar when the flow rate is close to 8 L/min. Tree-parallel insert and Plain insert on the contrary, only suffer pressure loss close to 1.20 bar and 0.80 bar at similar flow rate.

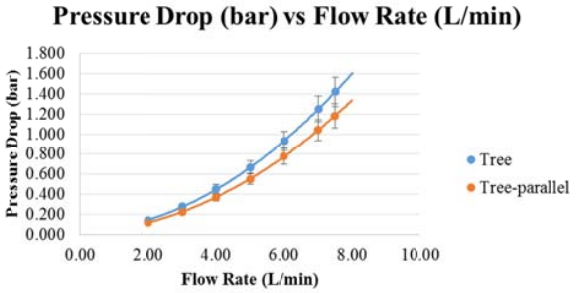

Fig. 13 Variation of pressure drop with flow rate

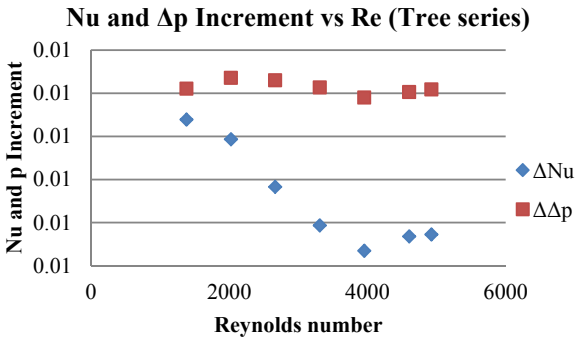

Fig. 14 Comparison of tree series based on heat transfer enhancement and pressure drop

The performance of Tree insert is compared to Tree-parallel in Fig. 14. Both the heat transfer coefficient and pressure drop induced by Tree insert is normalised by the corresponding parameters incurred by Tree-parallel insert. The pressure drop incurred by Tree insert is almost consistently higher than that of Tree-parallel at about 20 percent. The enhancement in terms of heat transfer coefficient is comparable to pressure drop increment in the laminar region, with a value of 16 percent at low Re. It then deteriorates at high Reynolds, with less than 5 percent improvement at Re values exceeding 3000.

Although results suggest desirable results at low Reynolds number, it is not economical to have tree design as the tree-parallel design can save more energy in terms of pumping power requirement, with just a slight drop in heat enhancement efficiency. Furthermore, the fabrication of the tree profile is effort and time consuming. The flow details are discussed to provide an insight on the probable causes and clue for further improvement.

The simulation results serve to explain the mechanism for the heat transfer enhancement and pressure drop by providing information such as flow paths, velocity distribution, and turbulence kinetic energy. All the results shown are based on 4 L/min flow rate at a heat supply of 1000 W.

Fig. 15 shows the streamlines on the surface of Tree insert whereas Fig. 16 shows the streamlines on the surface of Tree-parallel insert.

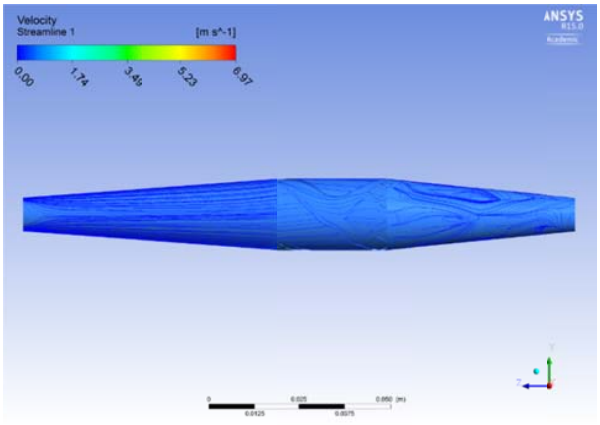

Fig. 15 Streamlines on the surface of tree insert

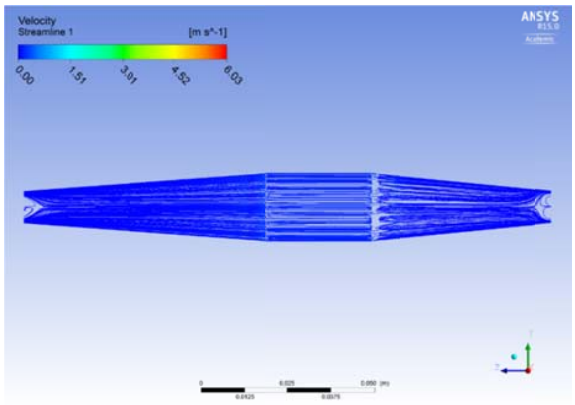

Fig. 16 Streamlines on the surface of tree-parallel insert

At 4 L/min at a heat supply of 1000W, both the heat transfer coefficient and pressure drop for Tree insert are slightly higher than that of Tree-parallel insert. As seen from Fig. 15, the fluid flows through longer path on the surface of Tree insert as compared to the Tree-parallel in Fig. 16. The longer path allows more heat exchange to take place, but at the same time, induces more pressure drop as expected. At the same time, the flow in the parallel channels is less perturbed. The grooves that form the channel extend from the start to the end of the heating region, thus regeneration of boundary layer is not significant, accounting for the low *h* and low friction factor. Fig. 17 and Fig. 18 show the turbulence kinetic energy for Tree insert and Tree-parallel insert respectively.

Fig. 17 Turbulence kinetic energy for Tree insert

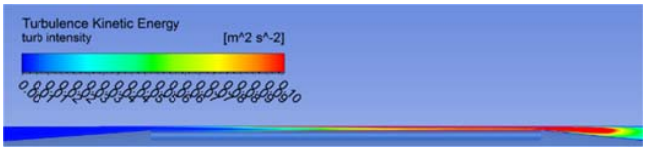

Fig. 18 Turbulence kinetic energy for Tree-parallel insert

The turbulence kinetic energy for Tree insert is high along the length as shown in Fig. 17. The turbulence kinetic energy for the Tree-parallel becomes higher only near the end of the channel, as depicted in Fig. 18. This is attributable to the variation in the fluid path of the microchannel along the length of the insert. Turbulent flows have higher heat transfer and thus higher pressure drop as discussed before.

B. Constructal Fin Series Insert

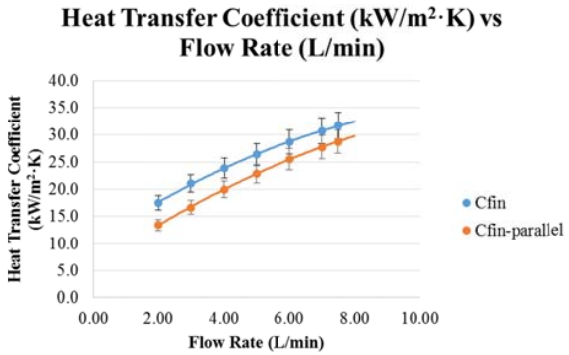

Fig. 19 Variation of Heat Transfer Coefficient with Flow Rate

Fig. 19 depicts the variation of heat transfer coefficients of Cfin series inserts with flow rate. The heat transfer coefficients increase with the flow rate, similar to that of Tree series inserts. The enhancement due to Cfin insert is very obvious in comparison to both Cfin-parallel and Plain inserts. The *h* value incurred by Cfin insert is around 17.5 kW/m^2·K even at a flow rate of 2 L/min. This value is about 75 percent higher than that incurred by Plain insert. The *h* value incurred by Cfin insert exceeds 30 kW/m^2·K at 8 L/min flow rate.

As compared to Cfin-parallel insert, the enhancement of *h* by Cfin insert deteriorates as flow rate increases, as the *h* values for both inserts fall into each other's uncertainty range beyond flow rate of 5 L/min. Similar trend is manifested for the dimensionless numbers as shown in Fig. 20. At low Reynolds number, Cfin insert manifests very clear enhancement in heat transfer coefficient as compared to both Cfin-parallel and Plain inserts.

The plot of variation of pressure drop with flow rate for Cfin series inserts, as shown in Fig. 21, indicates the hydrodynamic performance of these inserts. As noted from the graph, the pressure drop for the inserts increases with flow rate, in accordance with the conventional theory. It is noteworthy that the pressure drop for both Cfin and Cfin-parallel inserts is very close, falling into the range of uncertainty even at low flow rates. Although the pressure drop for Cfin and Cfin-parallel inserts is close to 1.50 bar at 8

L/min flow rate, it is easily tackled by a commercially available pump.

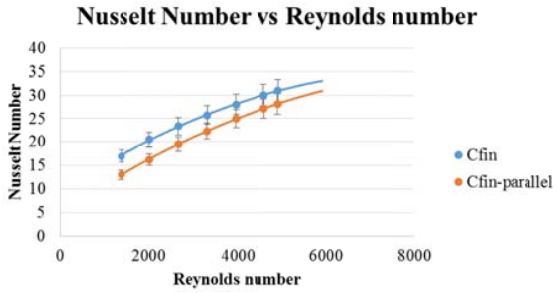

Fig. 20 Variation of Nusselt number with Reynolds number

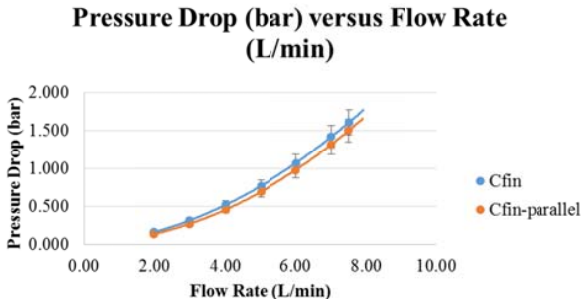

Fig. 21 Variation of Pressure Drop with Flow Rate

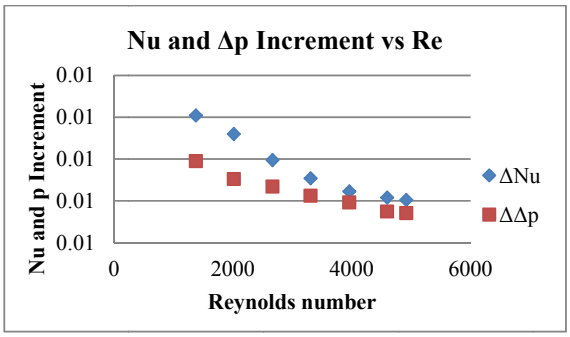

Fig. 22 Variation of Nusselt number with Reynolds number

The heat transfer and hydrodynamic performance of Cfin insert is compared to that of Cfin-parallel insert in Fig. 22. The performance of Cfin insert meets the objective of the project, which is to achieve a relatively lower increase in pressure drop as compared to the increment in heat transfer. The Nusselt number increment is always higher than the increment in pressure drop at all Reynolds numbers, more significantly at lower Reynolds number. At Reynolds number of 1000, the Nusselt number caused by Cfin insert is 30 percent more than that of the Cfin-parallel insert. Yet the increase in pressure drop is merely 20 percent. In other words, the Cfin insert achieves energy saving if compared to Cfin-parallel insert. This is a significant breakthrough as this trend was not observed by some studies [4], [8].

As suggested by studies [16], [17] , the bifurcation helps to recover the pressure loss. The tapered increase in cross sectional area at the junction is akin to a diffuser. The pressure recoveries at the bifurcation compensate the pressure drop due to reinitialisation of boundary layers and turbulence regime.

The irregularities of the surface of Cfin insert are relatively much higher than other inserts. This design reinitiates the development of boundary layers, another heat transfer enhancing mechanism. The average heat transfer coefficient in the developing region is higher than the developed region as shown in the previous section.

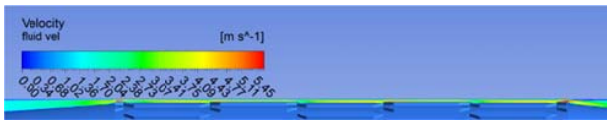

Fig. 23 Fluid velocity on the surface of Cfin insert

The high heat transfer coefficient attained by Cfin insert is mainly due to the discontinuous grooves found on the surface of the insert. It can be seen from Fig. 23 that there are regenerations of boundary layers due to the change in velocity magnitude along the length of the insert. On the contrary, the flow is fully developed for the case of Cfin-parallel insert. The velocities in the Cfin-parallel microchannel remain relatively constant as shown in Fig. 24.

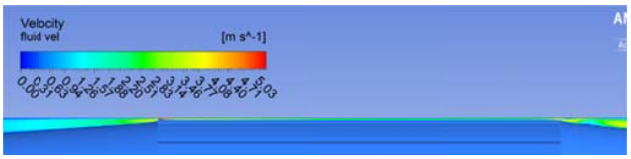

Fig. 24 Fluid velocity on the surface of Cfin-parallel insert

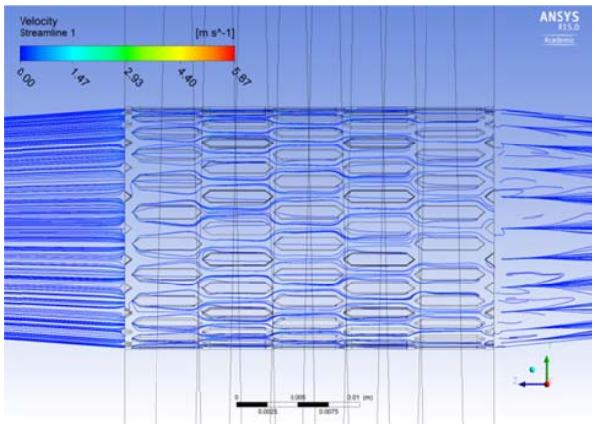

Fig. 25 Streamlines on the surface of Cfin insert

Although perturbed by the grooves on the surfaces, the channels formed by the Constructal fin have successfully bifurcated the flow to recover the pressure. The streamlines in Fig. 25 and Fig. 26 show how the flows are directed in the channels. It is obvious that the flows flowing through Cfin insert have been successfully bifurcated by the fins on the surface of the insert. On the contrary, the flows passing

through the Cfin-parallel insert are in straight lines as shown in Fig. 26.

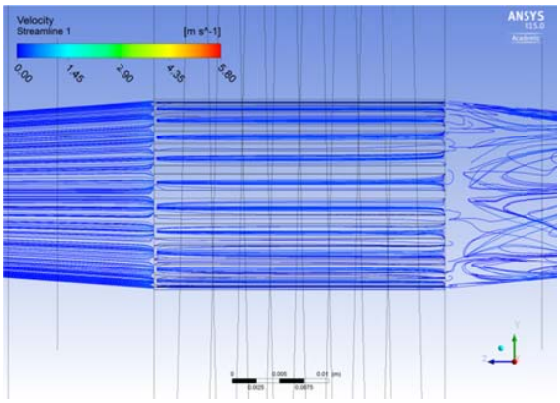

Fig. 26 Streamlines on the surface of Cfin-parallel insert

V. Conclusion

In conclusion, the Constructal features introduced on the surface of the insert improved the hydrodynamic and heat transfer performance of microchannel in macro geometry, particularly at low flow rates. Insert surfaces with Constructal features yielded high heat transfer coefficients as compared to surfaces with parallel channels.

Tree insert yielded the highest heat transfer coefficient of 30 kW/m^2·K at flow rate of 8 L/min. Overall, the Tree insert incurred better heat transfer enhancement as compared to Tree-parallel insert, owing to the longer flow path and more flow re-initialisations.

Cfin insert on the other hand, incurred lower pressure drop increment and higher heat transfer enhancement compared to Cfin-parallel insert. At low flow rate of 2 L/min, the heat transfer increment reached 30 percent at only a 20 percent increment in pressure drop. At high flow rate of 8 LPM, the heat transfer enhancement was comparable to the increase in pressure drop. Cfin insert had superior performance over Cfin-parallel insert in terms of heat transfer, attributable to more surface irregularities to reinitiate boundary layer redevelopment and higher turbulence kinetic energy. Although these processes also caused higher pressure drop, the bifurcation induced by the Constructal fins promoted pressure recoveries. The pressure recovery exceeded that generated by the heat transfer enhancing mechanisms, resulting in the relative lower pressure drop increment caused by Cfin insert as compared to Cfin-parallel insert.

VI. Recommendations and Future Work

The dimensioning of the Tree insert did not follow strictly to the Constructal design procedure owing to the limitation of CNC machining and the fixed microchannel size. Only some rules and principles were applied to the design of the tree surface profiles, hence the design was not comprehensive enough. Hence it is recommended that future work considers flow condition, heating condition and geometrical dimensions of the microchannel to fully tap into the application of Constructal theory. On the other hand, insert with Constructal fins showed a very promising direction for researchers to work on. The heat transfer had been successfully augmented using the grooves. The bifurcation angle of 75 degree managed to reduce the pressure drop at a percentage that is higher than the increment induced by the disturbance to the flow. The implementation of various angles of bifurcation is necessary to prove the robustness of the Constructal design. Furthermore, optimizing the geometries of the fins should be the highlight of future work.

References

[1] Tuckerman, D.B. and R. Pease, *High-performance heat sinking for VLSI.* Electron Device Letters, IEEE, 1981. 2(5): p. 126-129.
[2] Garimella, S.V. and C. Sobhan, *Transport in microchannels-a critical review.* Annual review of heat transfer, 2003. 13(13).
[3] Phillips, R.J., *Forced-convection, liquid-cooled, microchannel heat sinks*. 1988, DTIC Document.
[4] Kong, K.S. and K.T. Ooi, *A numerical and experimental investigation on microscale heat transfer effect in the combined entry region in macro geometries.* International Journal of Thermal Sciences, 2013. 68: p. 8-19.
[5] Mohammed, H., P. Gunnasegaran, and N. Shuaib, *Numerical simulation of heat transfer enhancement in wavy microchannel heat sink.* International Communications in Heat and Mass Transfer, 2011. 38(1): p. 63-68.
[6] Sui, Y., et al., *Fluid flow and heat transfer in wavy microchannels.* International Journal of Heat and Mass Transfer, 2010. 53(13): p. 2760-2772.
[7] Steinke, M.E. and S.G. Kandlikar. *Single-phase liquid heat transfer in plain and enhanced microchannels*. in *ASME 4th International Conference on Nanochannels, Microchannels, and Minichannels*. 2006. American Society of Mechanical Engineers.
[8] Goh, A.L., K.T. Ooi, and S. Ulrich, *Nature-inspired enhanced microscale heat transfer in macro geometry* in *2014 IEEE Intersociety Conference on Thermal and Thermomechanical Phenomena in Electronic Systems* 2014, IEEE: Orlando, FL p. 397-403.
[9] Bejan, A., *Constructal-theory network of conducting paths for cooling a heat generating volume.* International Journal of Heat and Mass Transfer, 1997. 40(4): p. 799-816.
[10] Wechsatol, W., S. Lorente, and A. Bejan, *Tree-shaped insulated designs for the uniform distribution of hot water over an area.* International Journal of Heat and Mass Transfer, 2001. 44(16): p. 3111-3123.
[11] Bejan, A. and S. Lorente, *Design with constructal theory.* 2008.
[12] Zhang, H., S. Lorente, and A. Bejan, *Vascularization with trees that alternate with upside-down trees.* Journal of Applied Physics, 2007. 101(9): p. 094904.
[13] Gosselin, L. and A. Bejan, *Tree networks for minimal pumping power.* International Journal of Thermal Sciences, 2005. 44(1): p. 53-63.
[14] Chen, Y., et al., *Thermal and hydrodynamic characteristics of constructal tree-shaped minichannel heat sink.* AIChE Journal, 2009: p. NA-NA.
[15] ANSYS, *ANSYS CFX-Solver Theory Guide* 2010, ANSYS Inc.
[16] Lee, Y.J., P.S. Lee, and S.K. Chou, *Numerical Study of Fluid Flow and Heat Transfer in the Enhanced Microchannel With Oblique Fins.* Journal of Heat Transfer, 2013. 135(4): p. 041901.
[17] Alharbi, A.Y., D.V. Pence, and R.N. Cullion, *Fluid Flow Through Microscale Fractal-Like Branching Channel Networks.* Journal of Fluids Engineering, 2003. 125(6): p. 1051.